Journal of Alzheimer's Disease 89 (2022) 39–49
DOI 10.3233/JAD-220024
IOS Press

Does Loss of Integrity of the Cingulum Bundle Link Amyloid-β Accumulation and Neurodegeneration in Alzheimer's Disease?

Naomi Vlegels[a,*], Rik Ossenkoppele[b,c], Wiesje M. van der Flier[b,d], Huiberdina L. Koek[e], Yael D. Reijmer[a], Laura EM Wisse[f], Geert Jan Biessels[a] and the Alzheimer's Disease Neuroimaging Initiative[1]

[a]*Department of Neurology, UMC Utrecht Brain Center, University Medical Center Utrecht, Utrecht University, Utrecht, The Netherlands*
[b]*Alzheimer Center Amsterdam, Department of Neurology, Amsterdam Neuroscience, Vrije Universiteit Amsterdam, Amsterdam UMC, Amsterdam, The Netherlands*
[c]*Clinical Memory Research Unit, Lund University, Lund, Sweden*
[d]*Department of Epidemiology and Data Science, VU University Medical Center, Amsterdam, The Netherlands*
[e]*Department of Geriatrics, University Medical Center Utrecht, Utrecht, The Netherlands*
[f]*Department of Diagnostic Radiology, Lund University, Lund, Sweden*

Handling Associate Editor: Jennifer Whitwell

Accepted 10 June 2022
Pre-press 11 July 2022

Abstract.
Background: Alzheimer's disease is characterized by the accumulation of amyloid-β (Aβ) into plaques, aggregation of tau into neurofibrillary tangles, and neurodegenerative processes including atrophy. However, there is a poorly understood spatial discordance between initial Aβ deposition and local neurodegeneration.
Objective: Here, we test the hypothesis that the cingulum bundle links Aβ deposition in the cingulate cortex to medial temporal lobe (MTL) atrophy.
Methods: 21 participants with mild cognitive impairment (MCI) from the UMC Utrecht memory clinic (UMCU, discovery sample) and 37 participants with MCI from Alzheimer's Disease Neuroimaging Initiative (ADNI, replication sample) with available Aβ-PET scan, T1-weighted and diffusion-weighted MRI were included. Aβ load of the cingulate cortex was measured by the standardized uptake value ratio (SUVR), white matter integrity of the cingulum bundle was assessed by mean diffusivity and atrophy of the MTL by normalized MTL volume. Relationships were tested with linear mixed models, to accommodate multiple measures for each participant.
Results: We found at most a weak association between cingulate Aβ and MTL volume (added R^2 <0.06), primarily for the posterior hippocampus. In neither sample, white matter integrity of the cingulum bundle was associated with cingulate Aβ or MTL volume (added R^2 <0.01). Various sensitivity analyses (Aβ-positive individuals only, posterior cingulate SUVR, MTL sub region volume) provided similar results.

*Correspondence to: Naomi Vlegels, Heidelberglaan 100, 3584 CX Utrecht, The Netherlands. Tel.: +31 88 75 568 66; E-mail: n.vlegels@umcutrecht.nl.

[1]Data used in preparation of this article were obtained from the Alzheimer's Disease Neuroimaging Initiative (ADNI) database (https://adni.loni.usc.edu/). As such, the investigators within the ADNI contributed to the design and implementation of ADNI and/or provided data but did not participate in analysis or writing of this report. A complete listing of ADNI investigators can be found at: https://adni.loni.usc.edu/wp-content/uploads/how_to_apply/ADNI_Acknowledgement_List.pdf

ISSN 1387-2877/$35.00

Conclusion: These findings, consistent in two independent cohorts, do not support our hypothesis that loss of white matter integrity of the cingulum is a connecting factor between cingulate gyrus Aβ deposition and MTL atrophy.

Keywords: Alzheimer's disease, amyloid-β, diffusion tensor imaging, medial temporal lobe, neurodegeneration, PET, white matter integrity

INTRODUCTION

Alzheimer's disease (AD) is characterized by the accumulation of amyloid-β (Aβ) into plaques, aggregation of tau into neurofibrillary tangles, and neurodegenerative processes like atrophy [1]. However, there is a notable spatial discordance between typical initial locations of Aβ deposition and neurodegenerative processes. Whereas Aβ deposition typically starts in the precuneus, medial orbitofrontal cortex, and the cingulate cortex [2, 3], the aggregation of tau and atrophy mostly starts in the medial temporal lobe (MTL) [4–6]. Additionally, while Aβ plaques are known to gradually spread throughout the brain, Aβ-PET studies have found relatively little involvement of Aβ in the MTL compared to neocortical regions [7–9]. This spatial discordance between Aβ deposition and neurodegeneration in the MTL in AD is poorly understood [10]. In addition, there is a largely unexplained temporal discordance, as Aβ deposition precedes neurodegenerative processes by a decade [11, 12].

A hypothesis in the AD field is that Aβ deposition and distant neurodegeneration might be interconnected through the functional and structural architecture of the brain [13]. If these two processes are indeed connected via the structural connections of the brain, i.e., the white matter tracts, the cingulum bundle is of particular interest, because it connects the typical starting locations of Aβ deposition (i.e., the cingulate cortex) with that of neurodegenerative processes (the MTL, see Fig. 1). The proposed role of the cingulum bundle could be two-fold. First, the cingulum might serve as a conduit for pathology or signals, linking Aβ deposition in the cingulate cortex to spread of tau and neurodegeneration from the MTL to the neocortex. Second, the tracts of the cingulum bundle might degenerate because of Aβ deposition on one end of the bundle, which might increase vulnerability of the MTL on the other end of the bundle and thereby promote local tau aggregation [14–17]. The integrity of the white matter in the cingulum bundle has been shown to be affected in AD [18] and has been implicated in Aβ-facilitated tau spread from the MTL to the posterior cingulate cortex [19].

In the current study, we explore the hypothesis that the cingulum bundle links Aβ deposition in the cingulate cortex to neurodegeneration in the MTL. We tested this hypothesis in early symptomatic disease stages, i.e., patients with mild cognitive impairment (MCI), by assessing whether the relationship between white matter integrity of the cingulum bundle and pathology at either end of the bundle (i.e., Aβ in the cingulate cortex and atrophy in the MTL) is stronger than the relationship between the two pathologies itself.

METHODS

Participants

UMCU

21 participants from the ABIDE study [20], recruited at the memory clinic of the UMC Utrecht (UMCU), were included. All participants underwent a one-day memory clinic evaluation including a physical examination, an interview, brain MRI and neuropsychological assessment. For the present study we selected participants with a diagnosis of MCI, available Aβ [^{18}F]-florbetaben PET scan, diffusion MRI scan, and 3D-T1-weighted MRI scan. Clinical diagnosis was established at a multidisciplinary consensus meeting after the one-day memory clinic evaluation. MCI was defined as complaints or deterioration from prior functioning and objective evidence of impairment in at least one cognitive domain. Furthermore, daily living activities had to be normal or mildly impaired [21, 22].

ADNI

As a replication sample, we included 37 participants from the multicentric Alzheimer's Disease Neuroimaging Initiative (ADNI, phase 3, downloaded August 2019 at https://adni.loni.usc.edu). We selected participants with a diagnosis of MCI who had an available Aβ [^{18}F]-florbetapir PET, available

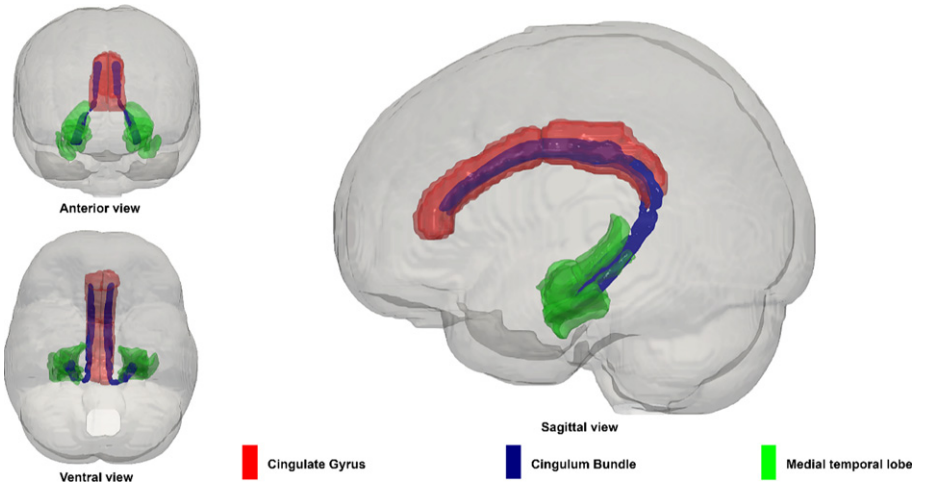

Fig. 1. Spatial overview of ROIs. A spatial overview of the cingulate gyrus (in red), the cingulum bundle (in blue) and the medial temporal lobe (in green) in anterior, ventral, and sagittal view.

diffusion MRI scan and available T1-weighted MRI (flowchart of the selection of participants can be found in Supplementary Figure 1). The MRI and PET scan had to be acquired with a maximum of 1 year apart. As diffusion measures are impacted by factors related to scanner and acquisition protocols [23–25], we selected participants from any center in which MRI was obtained on a Siemens scanner with a harmonized diffusion protocol. MCI diagnosis was based on the visit closest to the MRI scan. ADNI criteria for the diagnosis of MCI can be found on the website (https://adni.loni.usc.edu) and have been previously reported [26].

Neuroimaging

Amyloid PET

For the UMCU sample, Amyloid PET scans were made on a Siemens Biograph 40 MCT. Participants were injected with a tracer dose of approximately 300 MBq ± 20% [^{18}F]-florbetaben (NeuraceqTM). The image acquisition window extended from 90 to 110 min (4 × 5-min frames) after dose injection. Detailed information on acquisition and processing can be found in the Supplementary Methods. To obtain Aβ load for each participant, we first calculated the global cortical standardized uptake value ratio (SUVR) based on the volumes and the standardized uptake value (SUV) of all cortical ROIs with cerebellar gray matter as the reference tissue. For the primary analyses we used a composite score of the cingulate cortex (Cingulate SUVR) based on the Hammers atlas [27]. This composite consisted of the SUVR of the anterior cingulate and the posterior cingulate. In a sensitivity analysis, we've also assessed the SUVR of only the posterior cingulate.

For the ADNI sample, participants were injected with 370 MBq ± 10% [^{18}F]Florbetapir. Images were acquired 50 to 70 min (4 × 5-min frames) after dose injection. Further details on acquisition and processing of [^{18}F]-Florbetapir PET have been described elsewhere and can be found on the website [28] (https://adni.loni.usc.edu). As a global measure of Aβ load, we used the neocortical composite SUVR that comprises an average of frontal, cingulate, lateral-parietal, and lateral temporal gray matter regions-of-interest, using whole cerebellum as the reference region. For the primary analyses, we used the composite score of the cingulate regions (Cingulate SUVR) based on the Desikan-Killiany atlas [29] which consisted of the caudal anterior cingulate, isthmus cingulate, posterior cingulate and rostral anterior cingulate.

MRI acquisition

For the UMCU sample, brain MRI data was acquired using a Philips 3 T scanner (Achieva, Philips, Best, the Netherlands) with a standardized MRI protocol that included a 3D-T1 weighted sequence (192 continuous slices, voxel size: 1 × 1 × 1 mm^3, repetition time (TR)/echo time (TE): 7.9/4.5 ms, flip angle of 8°) and a diffusion-weighted sequence (single-shot echo EPI, 48 contiguous slices, voxel size 1.72 × 1.72 × 2.50 mm^3, TR/TE

6600/73 ms, 45 gradient directions with a b-value of 1200 s/mm^2 and one with a b-value of 0 s/mm^2 (number of signal averages = 3)).

For the ADNI sample, brain MRI data for participants included in this study was acquired using a Siemens 3 T scanner (Siemens Healthineers, Erlangen, Germany). The standardized MRI protocol included an MPRAGE (170 sagittal slices, voxel size of $1 \times 1 \times 1$ mm^3, TR/TE/Inversion time (TI): 2.98/2300/900 ms, flip angle of 9°) and a diffusion-weighted sequence (voxel size $2 \times 2 \times 2$ m^3, TR/TE: 7200/56, 41 gradient directions with a b-value of 1000 s/mm^2 and five with a b-value of 0 s/mm^2).

Diffusion preprocessing and tractography

For both the UMCU and ADNI study samples, the diffusion-weighted data was processed with ExploreDTI (version 4.8.6; https://www.exploredti.com/) [30] running on MATLAB R2018a (MATLAB and Statistics Toolbox Release 2014b, The MathWorks, Inc., Natick, Massachusetts, United States). Preprocessing of the data included correction for subject motion, eddy current and susceptibility artefacts, including rotation of the B-matrix prior to the estimation of the diffusion tensor [30–32]. The diffusion tensors were computed using robust estimators [31] followed by whole-brain tractography. Fiber tracts were reconstructed by starting seed points uniformly throughout the data at 2 mm isotropic resolution with a step size of 1 mm. Each streamline was propagated using integration over fiber orientation distributions. Streamlines were guided by fiber orientations inferred using constrained spherical deconvolution with a maximum harmonic order (*l-max*) of 6. This method allows for the reconstruction of more complex pathways, such as crossing fibers [33]. Streamlines were terminated when they entered a voxel with fiber orientation distributions <0.1 or when the deflection angle between two successive steps was >45°.

Following preprocessing and tractography, we manually reconstructed the superior part and the parahippocampal part of the cingulum bundle per hemisphere in each participant. For the reconstruction of the tracts we used an earlier described multiple region of interest (ROI) approach [34, 35]. In short, ROIs for tract selection and tract exclusion were manually drawn on color coded fiber orientation maps in native space. ROI placement was based on previously defined anatomical landmarks to reduce subjectivity in fiber tracking [36]. Low inter- and intra-rater variability with this method has been demonstrated in previous studies [37, 38]. For the reconstructed cingulum bundles, mean diffusivity (MD) was determined for the primary analysis. As a sensitivity analysis, we also performed an along tract analysis. Along tract analysis allows to assess multiple data points throughout the bundle rather than only the mean of the entire bundle, giving a higher sensitivity to subtle changes [39]. Along with the tract analysis, we assessed 8 different data points along the reconstructed cingulum bundles (4 for the superior part and 4 for the parahippocampal part) and determined MD for each of these data points per hemisphere, per subject.

Medial temporal lobe volume

MTL volume was determined for each participant by using the Automatic Segmentation of Hippocampal Subfields (ASHS) software package. More specifically we used the atlas for the T1-weighted MRI [40, 41]. ASHS automatically segments anterior and posterior hippocampus as well as MTL cortical sub regions for both hemispheres. All segmentation results were visually inspected, manual edits were not needed. Following visual inspection, we combined the volumes of the anterior hippocampus, posterior hippocampus, entorhinal cortex, Brodmann area 35 and 36 (perirhinal cortex) and the parahippocampal cortex to obtain MTL volume. MTL volume was normalized by the intracranial volume for each participant. For the UMCU sample intracranial volume was obtained by probabilistic segmentations using MeVisLab (MeVis Medical Solutions AG, Bremen, Germany). For the ADNI sample, intracranial volume was obtained by segmentations using the Computational Anatomical Toolbox (CAT) 12 toolbox (version R1073, C. Gaser, Structural Brain Mapping Group, Jena University Hospital, Jena, Germany) for SPM version 12.

Statistical analysis

All statistical analyses were performed in R (version 3.5.1) [42] and statistical significance level was set at $\alpha = 0.05$. All associations were tested with linear mixed models. Linear mixed models were used (using the "lme4" package; [43]) because they allow for both within- and between-subject factors, thus accommodating the four measurements of the cingulum bundle for each subject (left superior, right superior, left parahippocampal and right parahippocampal), two measurements for both cingulate SUVR and MTL (left and right), as well as considering between-subjects factors such as age and sex.

Table 1
Participant characteristics

	UMCU ($n = 21$)	ADNI ($n = 37$)
Age, y	75.9 ± 6.5	75.6 ± 7.9
Female sex	8 (38)	15 (41)
MMSE	26 [3.5] (21–29)	27 [2] (23–30)
Aβ-positive	14 (67)	22 (59)
[^{18}F]-florbetaben global SUVR	1.49 [0.3] (1.17–2.34)	NA
[^{18}F]-florbetaben cingulate SUVR	1.68 [0.45] (1.26–2.47)	NA
[^{18}F]-florbetapir global SUVR	NA	1.29 [0.57] (0.86–2.28)
[^{18}F]-florbetapir cingulate SUVR	NA	1.35 [0.54] (0,92–2,31)
ICV in ml	1445 [191] (1101–1645)	1482 [217] (1067–1774)
TBV, % of ICV	68.7 [4, 9] (62.5–73.3)	72.1 (6.7) (63.5–82.7)
MTL volume, % of ICV	0.89 [0.13] (0.75–1.11)	0.96 [0.17] (0.66–1.22)
MD Superior Cingulum bundle 10^{-4} mm^2/s	7.61 [0.41] (7.22–9.07)	7.77 [0.31] (7.2–9.1)
MD Hippocampal Cingulum bundle 10^{-4} mm^2/s	10.1 [1.77] (7.9–12.6)	9.34 [1.38] (7.7–11.9)

^{18}F, fluorine-18; Aβ, amyloid-β; ICV, intracranial volume; MD, mean diffusivity; mm, millimeter; MMSE, Mini-Mental State Exam; MTL, medial temporal lobe; NA, not applicable; SUVR, standardized uptake value ratio; TBV, total brain volume. Data is presented as mean ± standard deviation, *n* (%) and median [interquartile range] (min – max).

The association between Cingulate SUVR and MTL volume was tested with a model that included Cingulate SUVR, hemisphere (left/right), age, and sex. The relationship between Cingulate SUVR and Cingulum MD was tested with a model that included MD of the cingulum, location (superior or parahippocampal), hemisphere, age, and sex. For the association between MTL volume and cingulum MD we included MD of the cingulum, location, hemisphere, age, and sex. For these main analyses, we report the standardized fixed effect (B), the 95% confidence interval, the *p*-value, and explained variance (R^{2-}) of the model without and with the variable of interest.

We performed the following *post-hoc* sensitivity analyses (also with linear mixed models). First, all analyses were repeated in Aβ-positive individuals only, to rule out that findings were confounded by patients without AD pathology. For Aβ load we repeated the analysis with posterior cingulate cortex SUVR only, as this region is part of the posterior MTL network and might be more sensitive. For the integrity of the cingulum bundle we also ran a more fine-grained along tract analysis. For MTL volume, we zoomed in on specific sub regions of the structure as these might be more sensitive than the complete volume. We assessed 1) posterior hippocampus volume, as this is spatially close to the cingulate cortex; 2) entorhinal cortex volume as the cingulum bundle projects mostly on this structure; and 3) parahippocampal cortex as this region is part of the posterior MTL network, together with the posterior cingulate. All sensitivity analyses were done in a similar way as described in the preceding paragraph. All tests were performed separately for the UMCU and ADNI sample.

RESULTS

Table 1 shows the characteristics of the participants of both the UMCU and the ADNI sample.

Cingulate SUVR: MTL volume

No association was found between Cingulate SUVR and MTL volume in both the UMCU sample (B(CI): –0.27 (–0.63 – 0.09), $p = 0.197$, R^2 in model without and with SUVR 0.30 and 0.35, respectively) and the ADNI sample (B(CI) = –0.03 (–0.34 – –0.29), $p = 0.88$, R^2 in model without and with SUVR was 0.013 and 0.014, respectively), see Table 2 and Fig. 2A and 2B.

In a sensitivity analysis that assessed posterior hippocampus volume, an association was found for the ADNI sample (B(CI) = –0.38 (–0.67 – –0.08), *Bonferonni corrected* $p = 0.045$), but not the UMCU sample (Supplementary Table 6). All other sensitivity analyses (in Aβ-positive individuals, using posterior cingulate SUVR and using entorhinal cortex and parahippocampal volume) yielded results similar to the main analysis (Supplementary Tables 4–6).

Associations with cingulum MD

The findings in Table 2 and Fig. 2C and 2D indicate that there was no association between Cingulate SUVR and Cingulum MD for either the UMCU

Table 2
Main linear mixed model results

	UMCU			ADNI		
	β (CI)	F (df)	*p*	β (CI)	F (df)	*p*
Cing. SUVR – MTL vol.	–0.27 (–0.63 – 0.09)	1.84 (1, 13.4)	0.2	–0.03 (–0.34 – 0.29)	0.02 (1, 36.8)	0.88
MD – Cing. SUVR	0.01 (–0.06 – 0.07)	0.03 (1, 48.2)	0.86	–0.01 (–0.03 – 0.01)	1.33 (1, 108.2)	0.25
MD – MTL volume	0.06 (–0.16 – 0.28)	0.24 (1, 44.4)	0.62	– 0.01 (–0.10 – 0.08)	0.06 (1, 111.3)	0.80

Shows the main results for the linear mixed models. Top row shows the results for the relationship between cingulate Aβ and MTL volume, middle row the results for cingulum MD and cingulate Aβ and the bottom row shows the results of the relationship between cingulum MD and MTL volume. Results are displayed as follows: the standardized fixed effects coefficients (β) plus 95% confidence intervals, the F-tests with the degrees of freedom (df) and the *p*-value for both the UMCU and ADNI study samples.

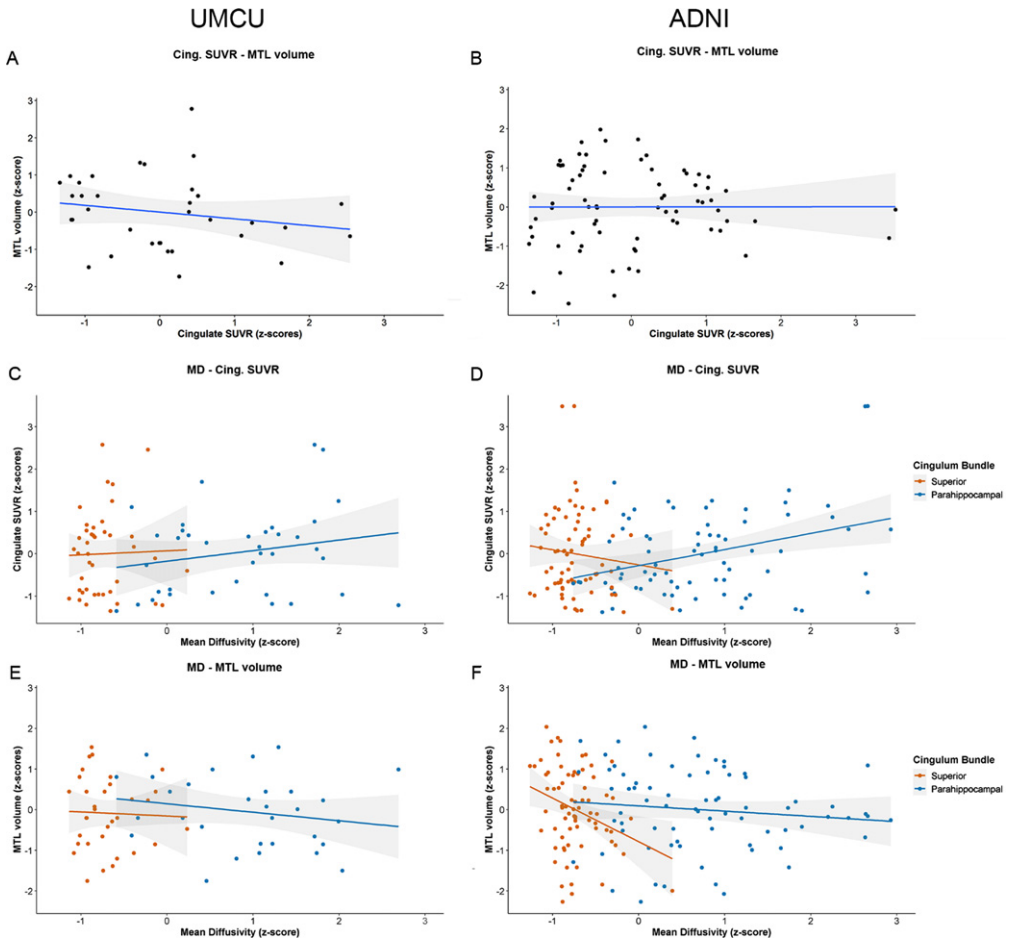

Fig. 2. Scatterplots of regression analyses. Scatterplots showing the association for UMCU (left) and ADNI (right) between Cingulate SUVR and MTL volume (A and B), for the association between Cingulum MD and Cingulate SUVR (C and D) as well as for the association between Cingulum MD and MTL volume. The legends on the outer right side of the figure refer to both panels.

(B(CI) = 0.006 (–0.06 – 0.07), $p = 0.86$, R^2 for model without or with SUVR was 0.0231 and 0.0232, respectively) or the ADNI sample (B(CI) = 0.013 (–0.03 – 0.01), $p = 0.25$, R^2 for model without or with SUVR was 0.017 and 0.017, respectively). There were no significant associations for any of the covariates: age, sex, hemisphere, and location (Supplementary Table 2). We performed sensitivity analyses in which we assessed the relationship between Cingulate SUVR and Cingulum MD in Aβ-positive individuals and in which we used posterior cingulate SUVR rather than Cingulate SUVR but both yielded no difference in results (Supplementary Tables 4 and 5).

There was no relationship between MTL volume and cingulum MD in either the UMCU (B(CI) = 0.06 (–0.16 – 0.28), $p = 0.62$, R^2 for model without and with MTL volume was 0.29 and 0.29, respectively) or the ADNI sample (B(CI) = –0.01(–0.10 – 0.08), $p = 0.80$, R^2 for model without and with MTL volume was 0.0077 and 0.0078, respectively), see Table 2 and Fig. 2E and 2F. There was no effect from the covariates (Supplementary Table 3). The sensitivity analysis in Aβ-positive individuals gave similar results (Supplementary Table 4). When we tested the association using volumes of the sub regions of the MTL rather than the complete MTL, results remained non-significant (Supplementary Table 6).

As a sensitivity analysis on the white matter integrity of the cingulum, we performed a more fine-grained along-tracts analysis of 8 data points of the MD of the cingulum bundle. This analysis did not change the interpretation of the results (data not shown).

DISCUSSION

We found at most a weak association between Cingulate Aβ and MTL volume, primarily for the posterior hippocampus, in line with earlier findings [36, 37]. In neither sample, white matter integrity of the cingulum bundle was associated with Cingulate Aβ on one end of the bundle or MTL volume at the other end. These consistent findings in two independent cohorts of patients with MCI do not support our hypothesis that loss of integrity of the cingulum bundle links Aβ deposition in the cingulate cortex to neurodegeneration of structures in the MTL.

Aβ deposition, tau aggregation and neurodegeneration are all characteristic features of AD, but Aβ deposition has a striking spatiotemporal discordance with tau and neurodegeneration [17, 44]. The temporal discordance has been attributed to the sequence in which pathological processes take place. Aβ accumulates first while neurodegeneration starts about a decade later [11, 45]. By the time that neurodegeneration starts, Aβ deposition is believed to have reached a plateau level [44, 46], which in part explains the weak correlation between levels of biomarkers for these processes, as we also see in the current study. Here we focused on the discordant starting locations of Aβ deposition compared to tau and neurodegenerative processes and zoomed in on loss of white matter integrity of the cingulum bundle as a connecting factor. The cingulum bundle was primarily chosen because of its anatomical location, directly linking the cingulate gyrus and the MTL, but the bundle is also known to be affected in AD [18]. Microstructural changes in the cingulum bundle, specifically in the parahippocampal cingulum, are well established in MCI and AD [18, 47, 48]. Mito et al. [48] showed that the posterior cingulum bundle was 1 of 2 bundles affected in patients with MCI when compared to healthy controls. The integrity of the cingulum bundle has also been shown to predict tau deposition in the posterior cingulate cortex in Aβ positive individuals from the MTL to the posterior cingulate cortex [19].

This study did not find that Aβ deposition was linked to atrophy in the MTL via loss of integrity of the cingulum bundle. For the primary analysis we deliberately looked at the cingulate cortex and the complete MTL. It could, however, be argued that looking at these ROIs in closer detail would reveal more subtle relationships. Nevertheless, the *post hoc* sensitivity analyses that we performed did not show such an effect, with the exception of the association between cingulate Aβ and posterior hippocampal volume. Our findings do not preclude involvement of white matter tracts in the dissemination of AD disease processes across the brain. Aβ in the neocortex might facilitate tau spread via the white matter tracts, without the tracts itself being damaged in that process [16]. A hint towards such a mechanism can be found in functional connectivity studies. It has been established in multiple studies that the default mode network, which shows reduced connectivity in AD, shows a large overlap with Aβ deposition patterns [49, 50]. Furthermore, network analysis has shown that the level of connectivity to an initially affected area is a more important factor for vulnerability to Aβ deposition than proximity to such an affected area [51–53].

The main strength of our study is that we performed a hypothesis-driven study in two independent cohorts of patients with MCI with high quality MRI and PET data. We used a state-of-the-art diffusion imaging analysis pipeline which included modern preprocessing techniques. One important aspect of diffusion MRI is that it is susceptible for scanner influences. For ADNI, a multicenter study, we tried to limit scanner influences on the diffusion measures by only selecting MRIs obtained on a Siemens scanner with a harmonized protocol. However, they were still obtained on different (types of) scanners which might have influenced our diffusion measures. Furthermore, the voxels of the UMCU diffusion scan were slightly

anisotropic, which might have negatively influenced tractography results. However, we found very similar results in the ADNI cohort for which the diffusion scan was isotropic.

Another limitation is that our study design did not include controls, meaning that we could not establish if the white matter integrity of the cingulum was indeed affected in patients, as would be expected based on the literature [48, 54]. However, when we compared whole white matter MD of the MCI patients from the UMCU to the MD of a healthy control group ($n = 47$) from one of our previous studies [55], MD was, as expected, significantly increased in the patient group (mean $\pm$ sd ($\times 10^{-4}$) patients: 8.21 ± 0.53; mean $\pm$ sd ($\times 10^{-4}$) controls: 7.81 ± 0.31). Furthermore, we assessed an MCI population and the lack of associations of both MTL atrophy and white matter integrity with Aβ deposition might be because of a plateau effect of this latter biomarker. However, the association between Aβ markers and atrophy is known to be inconsistent, also in early stages of the disease [56, 57] as is the association of Aβ markers with white matter integrity [58–60]. Another limitation is that we could only assess Aβ-PET as AD biomarker. Tau, especially in the entorhinal cortex, might have been valuable but this was not available for the UMCU sample. Lastly, in both cohorts sample sizes were modest, which affects statistical power. However, the results were very consistent across cohorts and point estimates for the tested associations were close to zero, indicating that the null finding is unlikely to be due to low power alone. Furthermore, future studies could use Bayesian models to exclude even small effects.

In conclusion, our results do not support the hypothesis that loss of integrity of the white matter is a connecting factor between Aβ deposition in the cingulate gyrus and local neurodegeneration in the MTL. The hypothesis on involvement of the white matter tracts in the dissemination of AD disease processes should be further explored in future studies with a larger group of Aβ-positive individuals.

ACKNOWLEDGMENTS

Part of the data used in preparation of this manuscript were obtained from the ADNI database. As such, the investigators within the ADNI contributed to the design and implementation of ADNI and/or the provided data but did not participate in analysis or writing of this report. A complete listing of the ADNI investigators can be found at http://adni.loni.usc.edu/wp-content/uploads/how_to_apply/ADNI_Acknowledgement_List.pdf.

Members of the Utrecht VCI study group involved in the present study (in alphabetical order by department): University Medical Center Utrecht, the Netherlands, Department of Neurology: E. van den Berg, J. M. Biesbroek, M. Brundel,W. H. Bouvy, L. G. Exalto, C. J. M. Frijns, O. Groeneveld, S. M. Heringa,R. Heinen, N. Kalsbeek, L. J. Kappelle, J. H. Verwer; Department of Radiology/Image Sciences Institute: J. de Bresser, H. J. Kuijf, A. Leemans, P.R.Luijten, M.A.Viergever, K.L.Vincken, J.J.M.Zwanenburg; Hospital Diakonessenhuis Zeist, the Netherlands: M. Hamaker, R. Faaij, M. Pleizier, E. Vriens.

Florbetaben scans of the UMCU cohort were made as part of the Dutch ABIDE project and supported by a ZonMW-Memorabel grant (project No 733050201), and through a grant of Piramal Imaging (PET scan costs). This work was also supported by ZonMw, The Netherlands Organisation for Health Research (VICI grant 91816616 to G.J. Biessels).

ADNI data collection and sharing was funded by the Alzheimer's Disease Neuroimaging Initiative (ADNI) (National Institutes of Health Grant U01 AG024904) and DOD ADNI (Department of Defense award number W81XWH-12-2-0012). ADNI is funded by the National Institute on Aging, the National Institute of Biomedical Imaging and Bioengineering, and through generous contributions from the following: AbbVie, Alzheimer's Association; Alzheimer's Drug Discovery Foundation; Araclon Biotech; BioClinica, Inc.; Biogen; Bristol-Myers Squibb Company; CereSpir, Inc.; Cogstate; Eisai Inc.; Elan Pharmaceuticals, Inc.; Eli Lilly and Company; EuroImmun; F. Hoffmann-La Roche Ltd and its affiliated company Genentech, Inc.; Fujirebio; GE Healthcare; IXICO Ltd.; Janssen Alzheimer Immunotherapy Research & Development, LLC.; Johnson & Johnson Pharmaceutical Research & Development LLC.; Lumosity; Lundbeck; Merck & Co., Inc.; Meso Scale Diagnostics, LLC.; NeuroRx Research; Neurotrack Technologies; Novartis Pharmaceuticals Corporation; Pfizer Inc.; Piramal Imaging; Servier; Takeda Pharmaceutical Company; and Transition Therapeutics. The Canadian Institutes of Health Research is providing funds to support ADNI clinical sites in Canada. Private sector contributions are facilitated by the Foundation for the National Institutes of Health (http://www.fnih.org).

The grantee organization is the Northern California Institute for Research and Education, and the study is coordinated by the Alzheimer's Therapeutic Research Institute at the University of Southern California. ADNI data are disseminated by the Laboratory for Neuro Imaging at the University of Southern California.

Authors' disclosures available online (https://www.j-alz.com/manuscript-disclosures/22-0024r2).

SUPPLEMENTARY MATERIAL

The supplementary material is available in the electronic version of this article: https://dx.doi.org/10.3233/JAD-220024.

REFERENCES

[1] Jack CR Jr, Bennett DA, Blennow K, Carrillo MC, Dunn B, Haeberlein SB, Holtzman DM, Jagust W, Jessen F, Karlawish J, Liu E, Molinuevo JL, Montine T, Phelps C, Rankin KP, Rowe CC, Scheltens P, Siemers E, Snyder HM, Sperling R, Elliott C, Masliah E, Ryan L, Silverberg N; Contributors (2018) NIA-AA Research Framework: Toward a biological definition of Alzheimer's disease. *Alzheimers Dement* **14**, 535–562.

[2] Iturria-Medina Y, Sotero RC, Toussaint PJ, Evans AC (2014) Epidemic spreading model to characterize misfolded proteins propagation in aging and associated neurodegenerative disorders. *PLoS Comput Biol* **10**, e1003956.

[3] Palmqvist S, Schöll M, Strandberg O, Mattsson N, Stomrud E, Zetterberg H, Blennow K, Landau S, Jagust W, Hansson O (2017) Earliest accumulation of β-amyloid occurs within the default-mode network and concurrently affects brain connectivity. *Nat Commun* **8** 1214.

[4] Jack CR Jr, Petersen RC, O'brien PC, Tangalos EG (1992) MR-based hippocampal volumetry in the diagnosis of Alzheimer's disease. *Neurology* **42**, 183-188.

[5] Whitwell JL, Petersen RC, Negash S, Weigand SD, Kantarci K, Ivnik RJ, Knopman DS, Boeve BF, Smith GE, Jack CR Jr (2007) Patterns of atrophy differ among specific subtypes of mild cognitive impairment. *Arch Neurol* **64**, 1130-1138.

[6] Pini L, Pievani M, Bocchetta M, Altomare D, Bosco P, Cavedo E, Galluzzi S, Marizzoni M, Frisoni GB (2016) Brain atrophy in Alzheimer's disease and aging. *Ageing Res Rev* **30**, 25-48.

[7] Cho SH, Shin JH, Jang H, Park S, Kim HJ, Kim SE, Kim SJ, Kim Y, Lee JS, Na DL, Lockhart SN, Rabinovici GD, Seong JK, Seo SW (2018) Amyloid involvement in subcortical regions predicts cognitive decline. *Eur J Nucl Med Mol Imaging* **45**, 2368-2376.

[8] Grothe MJ, Barthel H, Sepulcre J, Dyrba M, Sabri O, Teipel SJ (2017) *In vivo* staging of regional amyloid deposition. *Neurology* **89**, 2031-2038.

[9] Cho H, Choi JY, Hwang MS, Kim YJ, Lee HM, Lee HS, Lee JH, Ryu YH, Lee MS, Lyoo CH (2016) *In vivo* cortical spreading pattern of tau and amyloid in the Alzheimer disease spectrum. *Ann Neurol* **80**, 247-258.

[10] van der Kant R, Goldstein LSB, Ossenkoppele R (2020) Amyloid-β-independent regulators of tau pathology in Alzheimer disease. *Nat Rev Neurosci* **21**, 21-35.

[11] Jack CR, Knopman DS, Jagust WJ, Shaw LM, Aisen PS, Weiner MW, Petersen RC, Trojanowski JQ (2010) Hypothetical model of dynamic biomarkers of the Alzheimer's pathological cascade. *Lancet Neurol* **9**, 119-128.

[12] Baek MS, Cho H, Lee HS, Choi JY, Lee JH, Ryu YH, Lee MS, Lyoo CH (2020) Temporal trajectories of *in vivo* tau and amyloid-β accumulation in Alzheimer's disease. *Eur J Nucl Med Mol Imaging* **47**, 2879-2886.

[13] Raj A, Kuceyeski A, Weiner M (2012) A network diffusion model of disease progression in dementia. *Neuron* **73**, 1204-1215.

[14] Vogel JW, Iturria-Medina Y, Strandberg OT, Smith R, Levitis E, Evans AC, Hansson O (2020) Spread of pathological tau proteins through communicating neurons in human Alzheimer's disease. *Nat Commun* **11**, 2612.

[15] Bennett RE, DeVos SL, Dujardin S, Corjuc B, Gor R, Gonzalez J, Roe AD, Frosch MP, Pitstick R, Carlson GA, Hyman BT (2017) Enhanced tau aggregation in the presence of amyloid β. *Am J Pathol* **187**, 1601-1612.

[16] Raj A, Iturria-Medina Y (2019) Network spread models of neurodegenerative diseases. *Front Neurol* **9**, 1159.

[17] Jagust W (2018) Imaging the evolution and pathophysiology of Alzheimer disease. *Nat Rev Neurosci* **19**, 687-700.

[18] Metzler-Baddeley C, Jones DK, Steventon J, Westacott L, Aggleton JP, O'Sullivan MJ (2012) Cingulum microstructure predicts cognitive control in older age and mild cognitive impairment. *J Neurosci* **32**, 17612-17619.

[19] Jacobs HIL, Hedden T, Schultz AP, Sepulcre J, Perea RD, Amariglio RE, Papp KV, Rentz DM, Sperling RA, Johnson KA (2018) Structural tract alterations predict downstream tau accumulation in amyloid-positive older individuals. *Nat Neurosci* **21**, 424-431.

[20] de Wilde A, van Maurik IS, Kunneman M, Bouwman F, Zwan M, Willemse EA, Biessels GJ, Minkman M, Pel R, Schoonenboom NS, Smets EM, Wattjes MP, Barkhof F, Stephens A, van Lier EJ, Batrla-Utermann R, Scheltens P, Teunissen CE, van Berckel BN, van der Flier WM (2017) Alzheimer's biomarkers in daily practice (ABIDE) project: Rationale and design. *Alzheimers Dement (Amst)* **6**, 143-151.

[21] Petersen RC (2004) Mild cognitive impairment as a diagnostic entity. *J Intern Med* **256**, 183-194.

[22] Winblad B, Palmer K, Kivipelto M, Jelic V, Fratiglioni L, Wahlund LO, Nordberg A, Bäckman L, Albert M, Almkvist O, Arai H, Basun H, Blennow K, De Leon M, Decarli C, Erkinjuntti T, Giacobini E, Graff C, Hardy J, Jack C, Jorm A, Ritchie K, Van Duijn C, Visser P, Petersen RC (2004) Mild cognitive impairment – beyond controversies, towards a consensus: Report of the International Working Group on mild cognitive impairment. *J Intern Med* **256**, 240-246.

[23] Jones DK (2010) Precision and accuracy in diffusion tensor magnetic resonance imaging. *Top Magn Reson Imaging* **21**, 87-99.

[24] Vollmar C, O'Muircheartaigh J, Barker GJ, Symms MR, Thompson P, Kumari V, Duncan JS, Richardson MP, Koepp MJ (2010) Identical, but not the same: Intra-site and inter-site reproducibility of fractional anisotropy measures on two 3.0T scanners. *Neuroimage* **51**, 1384-1394.

[25] Grech-Sollars M, Hales PW, Miyazaki K, Raschke F, Rodriguez D, Wilson M, Gill SK, Banks T, Saunders DE, Clayden JD, Gwilliam MN, Barrick TR, Morgan PS, Davies NP, Rossiter J, Auer DP, Grundy R, Leach MO, Howe FA,

Peet AC, Clark CA (2015) Multi-centre reproducibility of diffusion MRI parameters for clinical sequences in the brain. *NMR Biomed* **28**, 468-485.

[26] Bondi MW, Edmonds EC, Jak AJ, Clark LR, Delano-Wood L, McDonald CR, Nation DA, Libon DJ, Au R, Galasko D, Salmon DP (2014) Neuropsychological criteria for mild cognitive impairment improves diagnostic precision, biomarker associations, and progression rates. *J Alzheimers Dis* **42**, 275-289.

[27] Hammers A, Allom R, Koepp MJ, Free SL, Myers R, Lemieux L, Mitchell TN, Brooks DJ, Duncan JS (2003) Three-dimensional maximum probability atlas of the human brain, with particular reference to the temporal lobe. *Hum Brain Mapp* **19**, 224-247.

[28] Landau SM, Fero A, Baker SL, Koeppe R, Mintun M, Chen K, Reiman EM, Jagust WJ (2015) Measurement of longitudinal β-amyloid change with 18F-florbetapir PET and standardized uptake value ratios. *J Nucl Med* **56**, 567-574.

[29] Desikan RS, Ségonne F, Fischl B, Quinn BT, Dickerson BC, Blacker D, Buckner RL, Dale AM, Maguire RP, Hyman BT, Albert MS, Killiany RJ (2006) An automated labeling system for subdividing the human cerebral cortex on MRI scans into gyral based regions of interest. *Neuroimage* **31**, 968-980.

[30] Leemans A, Jeurissen B, Sijbers J, Jones DK (2009) ExploreDTI: A graphical toolbox for processing, analyzing, and visualizing diffusion MR data. In *17th Annual Meeting of Intl Soc Mag Reson Med*, Hawaii, USA, p. 3537.

[31] Tax CMW, Otte WM, Viergever MA, Dijkhuizen RM, Leemans A (2015) REKINDLE: Robust Extraction of Kurtosis INDices with Linear Estimation. *Magn Reson Med* **73**, 794-808.

[32] Veraart J, Sijbers J, Sunaert S, Leemans A, Jeurissen B (2013) Weighted linear least squares estimation of diffusion MRI parameters: Strengths, limitations, and pitfalls. *Neuroimage* **81**, 335-346.

[33] Jeurissen B, Leemans A, Jones DK, Tournier JD, Sijbers J (2011) Probabilistic fiber tracking using the residual bootstrap with constrained spherical deconvolution. *Hum Brain Mapp* **32**, 461-479.

[34] Wisse LE, Reijmer YD, Ter Telgte A, Kuijf HJ, Leemans A, Luijten PR, Koek HL, Geerlings MI, Biessels GJ; Utrecht Vascular Cognitive Impairment (VCI) Study Group (2015) Hippocampal disconnection in early Alzheimer's disease: A 7 tesla MRI study. *J Alzheimers Dis* **45**, 1247-1256.

[35] Reijmer YD, Leemans A, Heringa SM, Wielaard I, Jeurissen B, Koek HL, Biessels GJ (2012) Improved sensitivity to cerebral white matter abnormalities in Alzheimer's disease with spherical deconvolution based tractography. *PLoS One* **7**, e44074.

[36] Catani M, Thiebaut de Schotten M (2008) A diffusion tensor imaging tractography atlas for virtual *in vivo* dissections. *Cortex* **44**, 1105-1132.

[37] Danielian LE, Iwata NK, Thomasson DM, Floeter MK (2010) Reliability of fiber tracking measurements in diffusion tensor imaging for longitudinal study. *Neuroimage* **49**, 1572-1580.

[38] Kristo G, Leemans A, De Gelder B, Raemaekers M, Rutten GJ, Ramsey N (2013) Reliability of the corticospinal tract and arcuate fasciculus reconstructed with DTI-based tractography: Implications for clinical practice. *Eur Radiol* **23**, 28-36.

[39] Colby JB, Soderberg L, Lebel C, Dinov ID, Thompson PM, Sowell ER (2012) Along-tract statistics allow for enhanced tractography analysis. *Neuroimage* **59**, 3227-3242.

[40] Yushkevich PA, Pluta JB, Wang H, Xie L, Ding SL, Gertje EC, Mancuso L, Kliot D, Das SR, Wolk DA (2015) Automated volumetry and regional thickness analysis of hippocampal subfields and medial temporal cortical structures in mild cognitive impairment. *Hum Brain Mapp* **36**, 258-287.

[41] Xie L, Wisse LEM, Das SR, Wang H, Wolk DA, Manjón J V, Yushkevich PA (2016) Accounting for the confound of meninges in segmenting entorhinal and perirhinal cortices in T1-weighted MRI. In *Medical Image Computing and Computer-Assisted Intervention – MICCAI 2016*, Ourselin S, Joskowicz L, Sabuncu MR, Unal G, Wells W, eds. Springer International Publishing, Cham, pp. 564-571.

[42] R Core Team (2018) R: A language and environment for statistical computing. R Foundation for Statistical Computing.

[43] Bates D, Mächler M, Bolker B, Walker S (2015) Fitting linear mixed-effects models using lme4. *J Stat Softw* **67**, 1-48.

[44] Jack CR Jr, Lowe VJ, Weigand SD, Wiste HJ, Senjem ML, Knopman DS, Shiung MM, Gunter JL, Boeve BF, Kemp BJ, Weiner M, Petersen RC (2009) Serial PIB and MRI in normal, mild cognitive impairment and Alzheimers disease: Implications for sequence of pathological events in Alzheimers disease. *Brain* **132**, 1355-1365.

[45] Caballero MÁ, Suárez-Calvet M, Duering M, Franzmeier N, Benzinger T, Fagan AM, Bateman RJ, Jack CR, Levin J, Dichgans M, Jucker M, Karch C, Masters CL, Morris JC, Weiner M, Rossor M, Fox NC, Lee JH, Salloway S, Danek A, Goate A, Yakushev I, Hassenstab J, Schofield PR, Haass C, Ewers M (2018) White matter diffusion alterations precede symptom onset in autosomal dominant Alzheimer's disease. *Brain* **141**, 3065-3080.

[46] Villemagne VL, Burnham S, Bourgeat P, Brown B, Ellis KA, Salvado O, Szoeke C, Macaulay SL, Martins R, Maruff P, Ames D, Rowe CC, Masters CL (2013) Amyloid β deposition, neurodegeneration, and cognitive decline in sporadic Alzheimer's disease: A prospective cohort study. *Lancet Neurol* **12**, 357-367.

[47] Bubb EJ, Metzler-Baddeley C, Aggleton JP (2018) The cingulum bundle: Anatomy, function, and dysfunction. *Neurosci Biobehav Rev* **92**, 104-127.

[48] Mito R, Raffelt D, Dhollander T, Vaughan DN, Tournier JD, Salvado O, Brodtmann A, Rowe CC, Villemagne VL, Connelly A (2018) Fibre-specific white matter reductions in Alzheimer's disease and mild cognitive impairment. *Brain* **141**, 888-902.

[49] Buckner RL, Snyder AZ, Shannon BJ, LaRossa G, Sachs R, Fotenos AF, Sheline YI, Klunk WE, Mathis CA, Morris JC, Mintun MA (2005) Molecular, structural, and functional characterization of Alzheimer's disease: Evidence for a relationship between default activity, amyloid, and memory. *J Neurosci* **25**, 7709-7717.

[50] Elman JA, Madison CM, Baker SL, Vogel JW, Marks SM, Crowley S, O'Neil JP, Jagust WJ (2016) Effects of beta-amyloid on resting state functional connectivity within and between networks reflect known patterns of regional vulnerability. *Cereb Cortex* **26**, 695-707.

[51] Zhou J, Gennatas ED, Kramer JH, Miller BL, Seeley WW (2012) Predicting regional neurodegeneration from the healthy brain functional connectome. *Neuron* **73**, 1216-1227.

[52] Sepulcre J, Grothe MJ, Sabuncu M, Chhatwal J, Schultz AP, Hanseeuw B, El Fakhri G, Sperling R, Johnson KA (2017)

Hierarchical organization of tau and Amyloid deposits in the cerebral cortex. *JAMA Neurol* **74**, 813-820.

[53] Pasquini L, Benson G, Grothe MJ, Utz L, Myers NE, Yakushev I, Grimmer T, Scherr M, Sorg C (2017) Individual correspondence of amyloid-β and Intrinsic connectivity in the posterior default mode network across stages of Alzheimer's disease. *J Alzheimers Dis* **58**, 763-773.

[54] Amlien IK, Fjell AM (2014) Diffusion tensor imaging of white matter degeneration in Alzheimer's disease and mild cognitive impairment. *Neuroscience* **276**, 206-215.

[55] Reijmer YD, Leemans A, Brundel M, Kappelle LJ, Biessels GJ, Group on behalf of the UVCI (VCI) S (2013) Disruption of the cerebral white matter network is related to slowing of information processing speed in patients with Type 2 diabetes. *Diabetes* **62**, 2112-2115.

[56] Becker JA, Hedden T, Carmasin J, Maye J, Rentz DM, Putcha D, Fischl B, Greve DN, Marshall GA, Salloway S, Marks D, Buckner RL, Sperling RA, Johnson KA (2011) Amyloid-β associated cortical thinning in clinically normal elderly. *Ann Neurol* **69**, 1032-1042.

[57] Chételat G, Villemagne VL, Bourgeat P, Pike KE, Jones G, Ames D, Ellis KA, Szoeke C, Martins RN, O'Keefe GJ, Salvado O, Masters CL, Rowe CC (2010) Relationship between atrophy and β-amyloid deposition in Alzheimer disease. *Ann Neurol* **67**, 317-324.

[58] Kantarci K, Schwarz CG, Reid RI, Przybelski SA, Lesnick TG, Zuk SM, Senjem ML, Gunter JL, Lowe V, Machulda MM, Knopman DS, Petersen RC, Jack CR (2014) White matter integrity determined with diffusion tensor imaging in older adults without dementia: Influence of amyloid load and neurodegeneration. *JAMA Neurol* **71**, 1547-1554.

[59] Vipin A, Ng KK, Ji F, Shim HY, Lim JKW, Pasternak O, Zhou JH (2019) Amyloid burden accelerates white matter degradation in cognitively normal elderly individuals. *Hum Brain Mapp* **40**, 2065-2075.

[60] Finsterwalder S, Vlegels N, Gesierich B, Araque Caballero M, Weaver NA, Franzmeier N, Georgakis MK, Konieczny MJ, Koek HL, Karch CM, Graff-Radford NR, Salloway S, Oh H, Allegri RF, Chhatwal JP, Jessen F, Düzel E, Dobisch L, Metzger C, Peters O, Incesoy EI, Priller J, Spruth EJ, Schneider A, Fließbach K, Buerger K, Janowitz D, Teipel SJ, Kilimann I, Laske C, Buchmann M, Heneka MT, Brosseron F, Spottke A, Roy N, Ertl-Wagner B, Scheffler K, Seo SW, Kim Y, Na DL, Kim HJ, Jang H, Ewers M, Levin J, Schmidt R, Pasternak O, Dichgans M, Biessels GJ, Duering M (2020) Small vessel disease more than Alzheimer's disease determines diffusion MRI alterations in memory clinic patients. *Alzheimers Dement* **16**, 1504-1514.